Sol−Gel Synthesis and Characterization of Co−Mo/Silica Catalysts for Single-Walled Carbon Nanotube Production

Veronica M. Irurzun, Yongqiang Tan, and Daniel E. Resasco*

School of Chemical Biological and Materials Engineering and Carbon Nanotube Technology Center (CANTEC), University of Oklahoma, 100 East Boyd Street, Norman, Oklahoma 73019

Received January 27, 2009. Revised Manuscript Received April 4, 2009

A series of silica-supported Co−Mo samples prepared by the sol−gel method has been compared as catalysts for the synthesis of single-walled carbon nanotubes (SWNT). The concentration ratio of ammonium hydroxide to the silica precursor tetraethoxysilane (TEOS) has an important effect on the resulting morphology of the silica support and, consequently, on the nature of the Co−Mo catalytic species. In turn, these morphology changes have significant effects on carbon yield, quality, and type of the single-walled carbon nanotubes obtained by the disproportionation of CO at 750 °C. In addition, a catalyst with an open microscale structure has been prepared by using carbon fibers as burnable sacrificial templates. This open structure results in several-fold enhanced carbon yield, while keeping the same nanotube quality as those obtained on conventional powder catalysts.

1. Introduction

The synthesis of single-walled carbon nanotubes (SWNT) with controlled structure by the CCVD (catalytic chemical vapor deposition) method is an area of great interest.[1−3] Extensive research efforts have been dedicated to control different aspects of their production such as selectivity, carbon yield, and overall quality. Our group has previously described the use of silica-supported Co−Mo catalysts (prepared by impregnation) for the production of SWNT by CO disproportionation, which forms the basis of the CoMoCAT process.[4] We have shown[5−11] that the yield and selectivity toward SWNT, as well as the overall nanotube quality, depend on operating conditions (e.g., temperature, pressure, gas composition) and catalyst preparation parameters (e.g., type of metal used, total loading, addition of a second metal, type of support).

In this contribution, a series of silica-supported Co−Mo catalysts prepared by the sol−gel method has been compared. The sol−gel method has been extensively used in the preparation of supported metal catalysts because it typically results in highly homogeneous materials with high degree of metal dispersion.[12−14] For example, Pd/SiO_2 catalysts prepared by the sol−gel method have not only exhibited higher surface area, narrower pore size distribution, and higher support thermal stability than impregnated catalysts but also higher resistance to metal particle sintering and lower deactivation during methane combustion.[15] Particularly relevant to the current work, this method has been also used to obtain active phases of Ni−Mo and Co−Mo[16] bimetallic catalysts supported on silica for the oxidative dehydrogenation of alkanes. It has been observed that catalysts prepared by the sol−gel method can stabilize the bimetallic active phases much more efficiently than those prepared by other methods. Therefore, sol−gel appears as a suitable method to produce $Co-Mo/SiO_2$ catalysts for the synthesis of SWNT, which requires stabilization of small clusters.

To obtain metal catalysts supported on high-surface area silica by the sol−gel method the polymerization of an alkoxy-silane such as tetraethoxysilane (TEOS), also known as tetraethyl orthosilicate, is carried out in the presence of the appropriate metal precursors.[17] When exposed to water, the alkoxy-silane hydrolyzes and, at different pH values, forms different monomeric species.[18] These species range from $[Si(OH)_3(OH_2)]^+$ at pH = 0 to $[SiO_2(OH)_2]^{2-}$ at pH = 14. Depending on the conditions, these species can condense and form oligomers at a different rate and with different configurations. To accelerate the polymerization, an increase in pH can be brought about by addition of a base, which

* To whom correspondence should be addressed. Phone: (405) 325-4370. E-mail address: resasco@ou.edu.

(1) Cassell, A. M.; Raymakers, J. A.; Kong, J.; Dai, H. J. *J. Phys. Chem. B* **1999**, *103*, 6484.
(2) Cheung, C. L.; Kurtz, A.; Park, H.; Lieber, C. M. *J. Phys. Chem. B* **2002**, *106*, 2429.
(3) Stanislav, A.; Moshkalev; Verissimo, C. *J. Appl. Phys.* **2007**, *102*, 1.
(4) Resasco, D. E.; Alvarez, W. E.; Pompeo, F.; Balzano, L.; Herrera, J. E.; Bitiyanan, B.; Borgna, A. *J. Nanopart. Res.* **2002**, *4*, 131.
(5) Herrera, J. E.; Balzano, L.; Borgna, A.; Alvarez, W. E.; Resasco, D. E. *J. Catal.* **2001**, *204*, 129.
(6) Alvarez, W.; Kitiyanan, B.; Borgna, A.; Resasco, D. E. *Carbon* **2001**, *39*, 547.
(7) Herrera, J. E.; Resasco, D. E. *J Phys. Chem. B.* **2003**, *107*, 3738.
(8) Herrera, J. E.; Resasco, D. E. *J. Catal.* **2003**, *221*, 354.
(9) Herrera, J. E.; Resasco, D. E. *Chem. Phys. Lett.* **2003**, *376*, 302.
(10) Bachilo, S. M.; Balzano, L.; Herrera, J. E.; Francisco, P.; Resasco, D. E.; Weisman, R. B. *J. Am. Chem. Soc.* **2003**, *125*, 11186.
(11) Lolli, G.; Zhang, L.; Balzano, L.; Sakulchaicharoen, N.; Tan, Y.; Resasco, D. E. *J. Phys. Chem. B.* **2006**, *110*, 2108.
(12) Meille, V. *Appl. Catal., A* **2006**, *315*, 1.
(13) Samanta, S.; Laha, S. C.; Mal, N. K.; Bhaumik, K. *J. Mol. Catal. A.* **2004**, *222*, 235.
(14) Delgado, M. R.; Arean, C. O. *J. Mater. Sci. Lett.* **2003**, *22*, 783.
(15) Pecchi, G.; Reyes, P.; Concha, I.; Fierro, J. L. G. *J. Catal.* **1998**, *179*, 309.
(16) Maione, A.; Devillers, M. *J. Solid State Chem.* **2004**, *177*, 2339.
(17) Klein, L. C. *Annu. Rev. Mater. Sci.* **1985**, *15*, 227.
(18) Henry, M.; Jolivet, J. P.; Livage, J. *Struct. Bonding (Berlin)* **1992**, *77*, 153.

10.1021/cm900250k CCC: $40.75
Published on Web 04/29/2009

causes a rapid hydrolysis followed by polymerization. Simultaneously with this polymerization process, the metal ions (e.g., Co and Mo) precipitate, thus forming a homogeneous and well dispersed mixture.

Previous studies by various authors[19,20] have shown that the final structure of the silica produced by sol−gel methods can be modified by varying preparation parameters such as type of alkoxide, pH of the medium (acidic or basic), water content, type of solvent, and process temperature. For example, it has been shown that the silica particle size increases with increasing concentration of alkoxide or ammonia as well as with increasing the length of the aliphatic chain in the solvent.[20] By contrast, the particle size decreases when water concentration or process temperature increases.[19] When the sol−gel method is used for the synthesis of supported metal catalysts, additional parameters related to the chemistry of the metal precursors are also important.

In this contribution, the effect of varying the ratio of the added ammonium hydroxide concentration has been studied, while keeping the other parameters constant. The concentration of ammonium hydroxide has an important effect on the rate of polymerization,[21] and consequently, we expect that it will affect significantly the resulting morphology. In addition, a catalyst with an open microscale structure was prepared by the sol−gel method, using a burnable sacrificial template which, after calcination, renders an open structure. This approach, known as sol−gel nanocoating, has been extensively employed by previous workers to prepare structured materials.[22] It gives us the opportunity to investigate the influence of the microstructure, while keeping the composition unchanged. The five catalysts prepared with varying structure were used to catalyze the growth of single-walled carbon nanotubes (SWNT) and to compare the resulting SWNT quality and yield.

2. Experimental Section

2.1. Catalysts Preparation and Characterization. Four different powder catalysts and a microscale structured catalyst were prepared by the sol−gel method. A constant total metal loading of 9 wt % of Co−Mo on SiO_2 (Co/Mo molar ratio of 1:3) was kept in all preparations. For the preparation of the powder catalysts, an aqueous solution of $Co(NO_3)_2 \cdot 6H_2O$ (Sigma Aldrich) was combined with an isopropanol solution of $MoCl_5$ (Sigma Aldrich). Then, mixtures of tetraethyl orthosilicate (TEOS) and ammonium hydroxide (28%) were added in different ratios. The corresponding samples are designated as AT(1/6), AT(2/6), AT(4/6), and AT(6/6), in which the numbers in parentheses indicate the volume ratio of ammonium hydroxide to TEOS. The four solutions were left to gel at room temperature for 20 h. The resulting colors of the gels were different for all samples, going from a dark orange to a light violet as the ammonia concentration increased. The gels were filtered and subsequently dried in air at 200 °C for 30 min and further calcined at 650 °C for 150 min.

To study the effect of incorporating a microscale structure in the sol−gel catalyst, we also prepared a microporous tubular-shaped supported catalyst by using a sol−gel preparation method and a tubular template. The tubular template used was a carbon fiber (cloth 3K) with diameter of 5−10 μm and cut in small pieces of about 5 mm long, purchased from Fiberlay, Inc. In this case, the metal precursor solutions and the TEOS were mixed together with the carbon fiber template before adding the ammonium hydroxide. The solution was left to gel at room temperature for 20 h, then filtered, subsequently dried at 200 °C for 30 min, and finally calcined at 650 °C for 150 min. It is important to mention that the sacrificial template was burnt during the calcination process, which resulted in an open tubular microstructure, as shown below.

The calcined catalysts were characterized by temperature-programmed reduction (TPR). The calcined samples were placed in a vertical quartz reactor and heated to 750 °C under He. After they were cooled down, the reduction of the oxide species under 20 sccm of a 5% H_2/Ar was measured.

Raman spectroscopy characterization of the catalyst samples was conducted in a Jovin Yvon-Horiba Laboratory Raman equipped with a CCD detector and with a laser excitation of 633 nm (He−Ne laser). The collection time was 60 s and three spectra from different spots were averaged for each sample. X-ray diffraction (XRD) characterization was conducted in Bruker AXS Discovery G8, equipped with a GADDS detector. The diffraction patterns were obtained for the catalysts preheated in He at 750 °C. The microscale structured catalyst was characterized by scanning electron microscopy (SEM) in a JSM-880 SEM microscope.

2.2. SWNT Growth and Product Characterization. The catalyst samples were previously reduced at 500 °C for 30 min under H_2 (125 sccm) in a 1/2 in. quartz reactor placed in a vertical furnace. After reduction, H_2 was switched to He (125 sccm) to reach the reaction temperature (750 °C). Later, the gaseous carbon source CO was passed over the reduced catalyst for 30 min at a flow rate of 250 sccm, while keeping the temperature at 750 °C. The system was finally cooled down under He flow. The same procedure was followed for the SWNT growing onto the microscale structured catalyst. The final product will be named as SWNT/catalyst indicating that the catalyst is still embedded with SWNT during some of the characterization techniques.

Raman characterization of the SWNT/catalyst product was conducted in the equipment mentioned above. The collection time in this case was 10 s, and three spectra from different spots on the sample were averaged for each product.

SWNT suspensions for optical absorption (OA) were prepared by ultrasonicating (Horn Sonic Dismembrator, Model 500, Fisher scientific) the SWNT/catalyst product in sodium cholate (20% (w/v) in deionized water (DI), Sigma Aldrich) for 60 min at 7 mW power. The suspension was then centrifuged (Dupont Sorvall SS-3) for 30 min at 15 000 rpm to separate the catalyst from the nanotubes. The supernatant liquid phase, which contains the nanotube suspended in surfactant, was collected for analysis in a Shimadzu UV-2101PC and a Bruker Equinox 55 FTNIR spectrophotometers.

The suspensions for transmission electron microscopy (TEM) analysis were prepared by suspending the SWNT/catalyst product by mild sonication in isopropanol.

Thermogravimetric analysis (TGA) was conducted in a TGAQ500 (TA Instruments Inc.) under an air flow at 200 °C for 15 min, and then it was heated up at a rate of 5 °C/min to 750 °C. Before each TGA measurement, the SWNT/catalyst product was first heated in air to 300 °C in an oven for 3 h to eliminate any potential amorphous carbon by oxidation (it is well-known that with the reversible CO disproportionation, the fraction of amorphous carbon

(19) Rahman, I. A.; Vejayakumaran, P.; Sipaut, C. S.; Isamil, J.; Abu Bakar, M.; Adnan, R.; Chee, C. K. *Colloids Surf., A* **2007**, *294*, 102.
(20) Mine, E.; Nagao, D.; Kobayashi, Y.; Konno, M. *J. Sol-Gel Sci Technol.* **2005**, *35*, 197.
(21) Brinker, C. J.; Sherer G. W. *Sol-Gel science: The physics and chemistry of sol-gel processing*; Academic press: New York, 1989.
(22) Caruso, R. A.; Antonietti, M. *Chem. Mater.* **2001**, *13*, 3272.

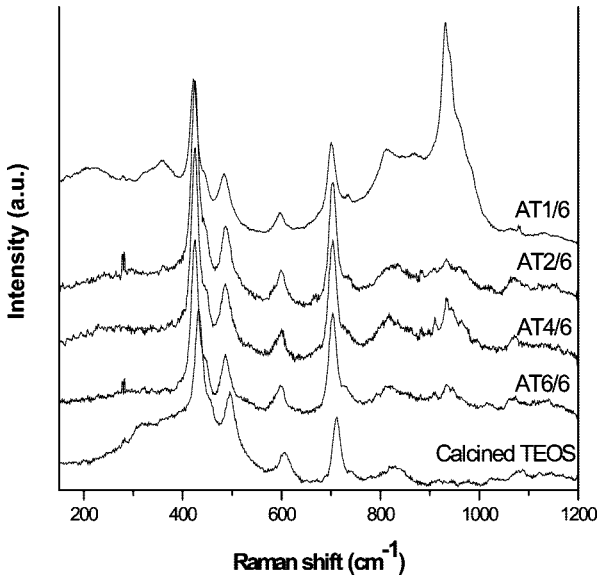

Figure 1. Raman spectra of four Co−Mo/SiO_2 powder calcined catalysts with ammonia/TEOS ratios from 1/6 to 6/6 compared with the spectra of pure calcined TEOS.

in the product is very low[6]). The dry powder product was stirred for several hours in aqueous solution of NH_4F_2 (Sigma Aldrich) to dissolve the silica support, filtered, and washed with DI water. Finally, it was treated with 35% HCl solution to dissolve the metal particles, further washed with DI water, filtered, and dried under vacuum for 2 days.

Temperature programmed oxidation (TPO) of the SWNT/catalyst product material using 80 sccm of 5% O_2 in He has been done to characterize the carbon species present in the samples.

Likewise, the SWNT/catalyst product obtained using the microscale structured catalyst was analyzed by scanning electron microscopy (SEM), Raman spectroscopy, TPO, and TGA.

3. Results and Discussion

3.1. Calcined Sol−Gel Powder Catalyst Series. *3.1.1. Raman Scattering.* Figure 1 shows the Raman spectra for the calcined powder catalyst samples. For comparison, the spectrum of a pure silica sample (calcined TEOS) is included. Without the presence of Co or Mo, the pure silica sample exhibits main bands at 431, 495, 606, and 713 cm^{-1}. As discussed in the literature[21−24] the peak at 431 cm^{-1} is related to the bending of Si−O−Si bonds, the peaks at 495 cm^{-1} and 606 cm^{-1} are related to the vibration of four-membered and three-membered silica rings, and the peak at 713 cm^{-1} is related to the symmetric stretching of the Si−O−Si bonds. Secondary bands are also observed at 820 cm^{-1} and are related to the symmetric stretching of the Si−O−Si bonds, the band at 978 cm^{-1} to the Si−OH stretching, and the band at 1076 cm^{-1} to the asymmetric stretching of the Si−O−Si bonds. On the other hand, the calcined Co−Mo/SiO_2 catalysts, in addition to the bands due to SiO_2, exhibit main peaks between 900 and 1000 cm^{-1}, which vary in intensity among the samples in the series. These bands are due to the Mo−O−Co stretching in α- and β-$CoMoO_4$ species,[16,25,26] with some contribution from bands corresponding to Mo oxides,[27] which is also present on the sample since Mo is in excess (i.e., Co/Mo = 1/3). The intensity of these bands provides a semiquantitative measurement of the presence of $CoMoO_4$ and Mo oxide crystallites. Specifically, while the intensity of these bands is very low and about the same for all the samples with an NH_4/TEOS ratio between 2/6 and 6/6, they are prominent for the sample with a ratio of 1/6, indicating the presence of larger crystals in this sample.

3.1.2. Temperature Programmed Reduction (TPR). The TPR profiles for three of the powder catalyst samples are summarized in Figure 2a. It can be seen that for the sample with the lowest NH_4OH/TEOS ratio AT(1/6), the H_2 consumption was significantly larger than those of the other catalysts. The rate of hydrogen consumption decreases after about 800 °C, about equally for the three catalysts. By contrast, for the other two, the hydrogen uptake is practically the same, while the maximum reduction peaks slightly shift to higher temperatures as the NH_4OH/TEOS ratio increases from AT(4/6) to AT(6/6).

Figure 2b shows the TPR profile of the AT(2/6) sample which reduces at lower temperatures than the other samples in the series but has about the same H_2 consumption as the samples with NH_4OH/TEOS ratios of 4/6 and 6/6. The differences in reducibility could be due to one of the following characteristics: (a) different degree of oxide crystallinity; (b) different CoMoOx compositions, or (c) different gas accessibility. A higher degree of crystallinity in the AT(6/6) sample, which would require a higher reduction temperature, should have been detected by Raman or XRD. In fact, sample AT(1/6) does show intense Raman bands confirming the presence of large Co molybdate crystals, but yet, the reduction does not shift to higher temperatures. Likewise, differences in composition as the NH_4OH/TEOS ratio increases could also cause an increment in reduction temperature if the clusters were more enriched in Mo. However, if this was the case, these oxides should have shown different Raman shifts for the different catalysts, but that is not the case. Therefore, we ascribe the increase in reduction temperature with increasing NH_4OH/TEOS ratio to lower accessibility, as Co and Mo species remain partially encapsulated by the silica support. The TPR profile for the open microstructure sample is included in Figure 2b as a comparison. It can be seen that the profile differs from the powder catalyst, and this difference may be related to the differences in structure, for example, gas accessibility.

For comparison, Figure 2c shows the TPR for the monometallic catalysts, Co/SiO_2 and Mo/SiO_2, prepared by the sol−gel method and the Co/SiO_2 and Mo/SiO_2 prepared by impregnation. It can be seen that Co reduces at higher

(23) Mayerhöfer, T. G.; Shen, Z.; Leonova, E.; Edén, M.; Kritz, A.; Popp, J. *J. Solid State Chem.* **2008**, *181*, 2442.
(24) Yuan, P.; He, H. P.; Wu, D. Q.; Wang, D. Q.; Chen, L. J. *Spectrochim. Acta A* **2006**, *60*, 2941.
(25) Resasco, D. E.; Herrera, J. E.; Balzano, L. *J. Nanosci. Nanotechnol.* **2004**, *4*, 1.
(26) Pawelec, B.; Halachev, T.; Olivas, A.; Zepeda, T. A. *Appl. Catal., A* **2008**, 30.
(27) Ohler, N.; Bell, A. T. *J. Catal.* **2005**, *231*, 115.

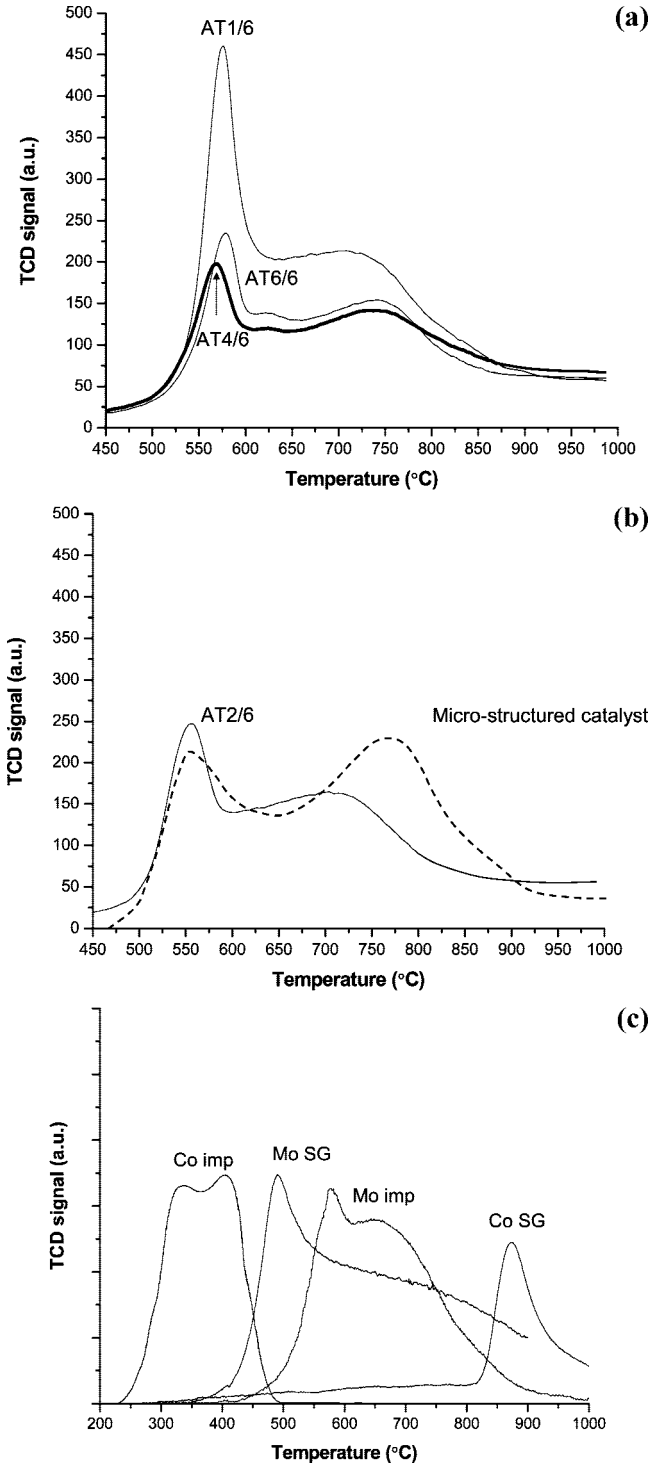

Figure 2. (a) TPR profiles of three Co−Mo/SiO_2 calcined powders with ammonia/TEOS ratios from 1/6 to 6/6. The samples were previously preheated in He to 750 °C. (b) TPR profile of a Co−Mo/SiO_2 calcined powders with ammonia/TEOS ratios from 2/6 and TPR profile of the microstructured catalyst. The samples were previously preheated in He to 750 °C. (c) TPR profiles of monometallic Co/SiO_2 and Mo/SiO_2 powder catalysts prepared by impregnation (imp) or using the sol gel method (SG). The samples were calcined and preheated in He to 750 °C before the TPR analysis was conducted.

temperatures on the sol−gel catalyst than the impregnated catalysts. As discussed above, this difference is due to the lower accessibility of Co on the samples prepared by sol−gel.

3.1.3. X-ray Diffraction (XRD). Figure 3 shows the diffractograms for the four powder catalysts obtained after

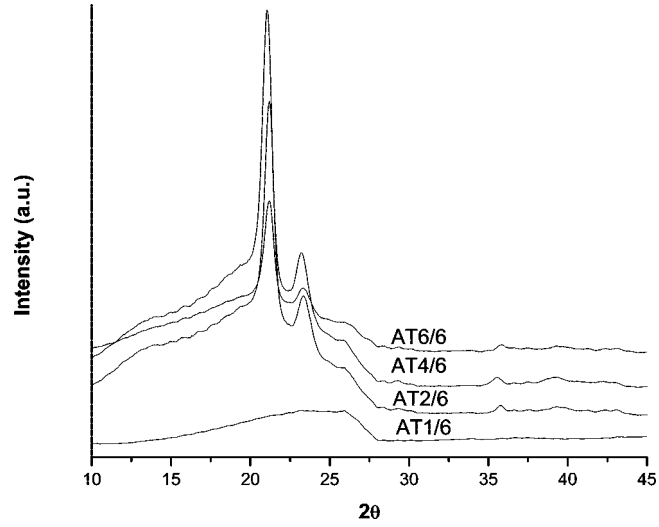

Figure 3. XRD difractograms of four Co−Mo/SiO_2 powder calcined catalysts with ammonia/TEOS ratios from 1/6 to 6/6. The samples were previously preheated in He to 750 °C.

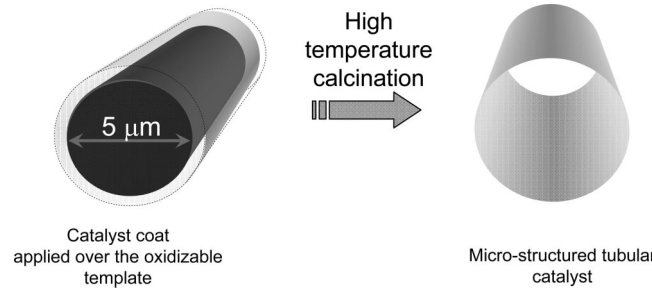

Figure 4. Schematic description of the microstructured catalyst preparation.

heating in He at 750 °C. Two sharp diffraction peaks are observed at 21° and 23°, and they can be ascribed to cristoballite-like and tridymite-like crystalline silica phases. It can be seen that increasing the NH_4OH/TEOS ratio from 1/6 to 6/6, the silica particles not only become larger but also more crystalline. These differences have not been seen in Raman because this is a shorter range analysis than XRD. The lack of crystallinity exhibited by the AT(1/6) can be due to the low extent of silica polymerization in the sample prepared with low ammonium content.

3.2. Calcined Sol−Gel Microscale Structured Catalyst. As illustrated schematically in Figure 4, the carbonaceous tubular template can be burnt away during calcination, leaving a tubular SiO_2 shell that preserves the shape of the sacrificial template, as shown in previous studies.[28,29]

3.3. SWNT Product Obtained on the Sol−Gel Powder and Microscale Structured Catalysts.

3.3.1. Optical Absorption (OA). The OA spectra for the nanotubes obtained on the different sol−gel powder catalysts and on the microscale structured catalyst are shown in Figure 5a,b, respectively. While the spectra of the product obtained on the powder catalysts show significant differences in absolute intensity from one catalyst to another, the relative intensities do not seem to vary significantly. By contrast a

(28) Zygmunt, J.; Krumeich, F.; Nesper, R. *Adv. Mater.* **2003**, *15*, 1538.
(29) Qian, H.; Yu, S. H.; Ren, L.; Yang, Y.; Zhang, W. *Nanotechnology* **2006**, *17*, 5995.

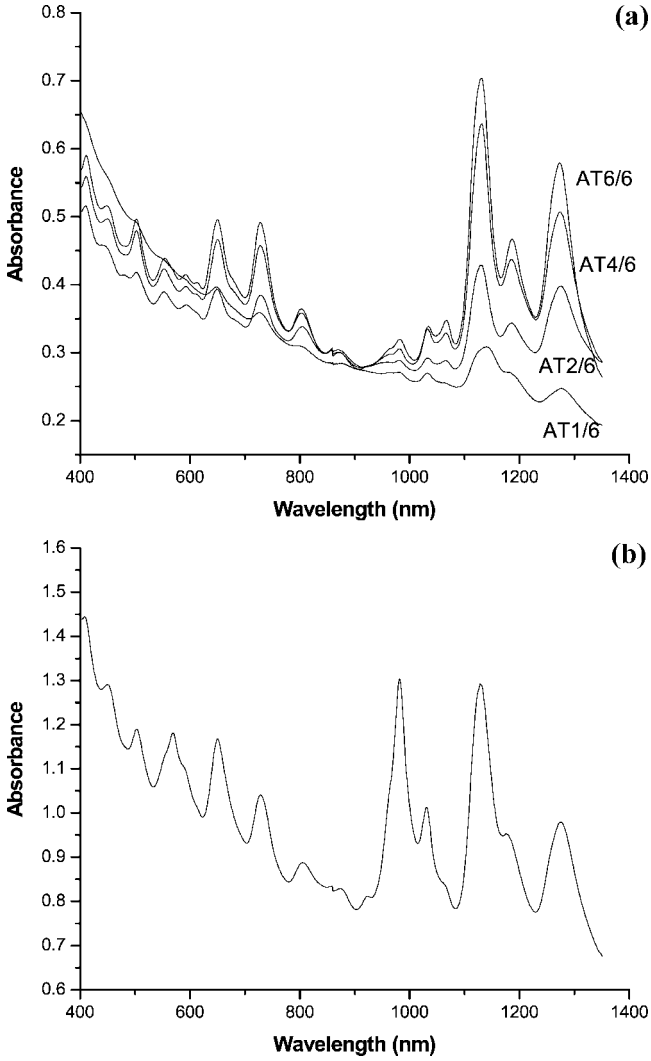

Figure 5. (a) OA spectra of SWNT grown onto four Co−Mo/SiO_2 powder catalysts with ammonia/TEOS ratios from1/6 to 6/6. (b) OA spectra of SWNT grown onto a Co−Mo/SiO_2 microstructured catalyst with an ammonia/TEOS ratio of 2/6.

broader distribution of SWNT species is apparent on the product obtained over the microscale structured catalyst, with high intensity in the region corresponding to small diameter semiconducting tubes. To quantify these variations an analysis of the different (*n*,*m*) species in each sample has been conducted. Table 1 shows the wavelength of the bands observed in the OA analysis together with (*n*,*m*) assignments for nanotubes that absorb near the observed wavelengths. Considering simultaneously the positions of both E_{11} and E_{22} transitions, we can accurately determine the (*n*,*m*) species in the product of the various catalysts. Accordingly, the stronger bands seen in Figure 5a for the powder catalysts can be assigned to the species (7,6) and (8,7). Lower concentrations of (6,5), (7,5), and (8,6) are also observed. Much weaker bands are consistent with the presence of (8,4), (12,1), (9,2), and (9,4) species. In contrast to the typical Co−Mo/SiO_2 catalyst prepared by impregnation and used in our standard CoMoCAT process, which yields to a product highly enriched in (6,5), the powder catalysts prepared in this work by the sol−gel method result in a broader distribution of chiralities. Figure 6a summarizes the distribution of the main chiralities for the different samples. It can

Table 1. (*n*,*m*) Assignments Using Observed Optical Absorption and Raman Bands of the SWNT Grown onto Co−Mo/SiO_2 Powder Catalysts

wavelength (nm) of observed optical absorption bands, E_{11}	wavelength (nm) of Observed optical absorption bands, E_{22}	(*n*,*m*) with E_{11} and E_{22} matching observed wavelengths	*d* (nm)
410		(5,5)	0.688
981	553	(6,5)	0.757
450		(6,6)	0.825
1033	649	(7,5)	0.829
1131	649	(7,6)	0.895
502		(7,7)	0.963
1131	594	(8,4)	0.84
1186	726	(8,6)	0.966
1271	726	(8,7)	1.032
553		(8,8)	1.1
1131	553	(9,2)	0.806
1066	726	(9,4)	0.916
1186	803	(12,1)	0.995

be observed that as the NH_4OH/TEOS ratio increases from 2/6 to 6/6 the average tubes diameters decreases. However, when the NH_4OH/TEOS ratio is the lowest (1/6) the synthesis of small diameter tubes is also favored. Figure 6b shows the intensity ratio between (8,7) and (7,6) species. It can be seen that sample AT(2/6) has the maximum (8,7)/(7,6) ratio.

Figure 6c shows the distribution of the different (*n*,*m*) SWNT types obtained onto the microscale structured catalyst. As mentioned above, a significant amount of SWNT of smaller diameter, for example, (6,5), is obtained, which is not seen on the powder catalysts.

The fraction of carbon nanotubes that remains in suspension after centrifugation has been calculated, and in all cases; it falls in the range of 30−60%.

3.3.2. Raman Scattering. Figure 7a,b shows the Raman spectra of the SWNT/catalyst product produced on the sol−gel powder, AT(1/6) to AT(6/6), and on the microscale structured catalysts, respectively. In these measurements, the samples were studied as produced, that is, with the catalyst still embedded in the SWNT product. As described in previous publications,[30] the Raman spectral region below 300 cm^{-1} is related to the radial breathing mode (RBM), the region between 1250 and 1450 cm^{-1} (D band) is ascribed to disordered carbon and structural defects of the tubes, and the strong band between 1540 and 1600 cm^{-1} (G band) is related to the graphene optical mode and is due to carbon atoms vibrations tangentially to the walls. The intensity ratios between the G and the D bands[31,32] have been typically used as nanotube quality indicators. The calculated G/D ratios are shown in Figure 8. In the sol−gel powder catalyst series, maxima in G/D values and carbon yields are obtained for the AT(2/6) sample. Increasing or decreasing the NH_4OH/TEOS ratio away from this optimum value results in losses for both the G/D ratio and carbon yield. In the case of the sol−gel microscale structured catalyst, the G/D value is as high as that of the best product, AT(2/6), from the powder catalyst series, but the carbon yield is much higher (24%). As anticipated, the open structure of the sol−gel microscale structured catalyst resulted in an enhanced SWNT yield.

3.3.3. Electron Microscopy (TEM and SEM). The TEM images in Figure 9a−c confirm that the samples with NH_4OH/TEOS ratios from 2/6 to 6/6 display high selectivity

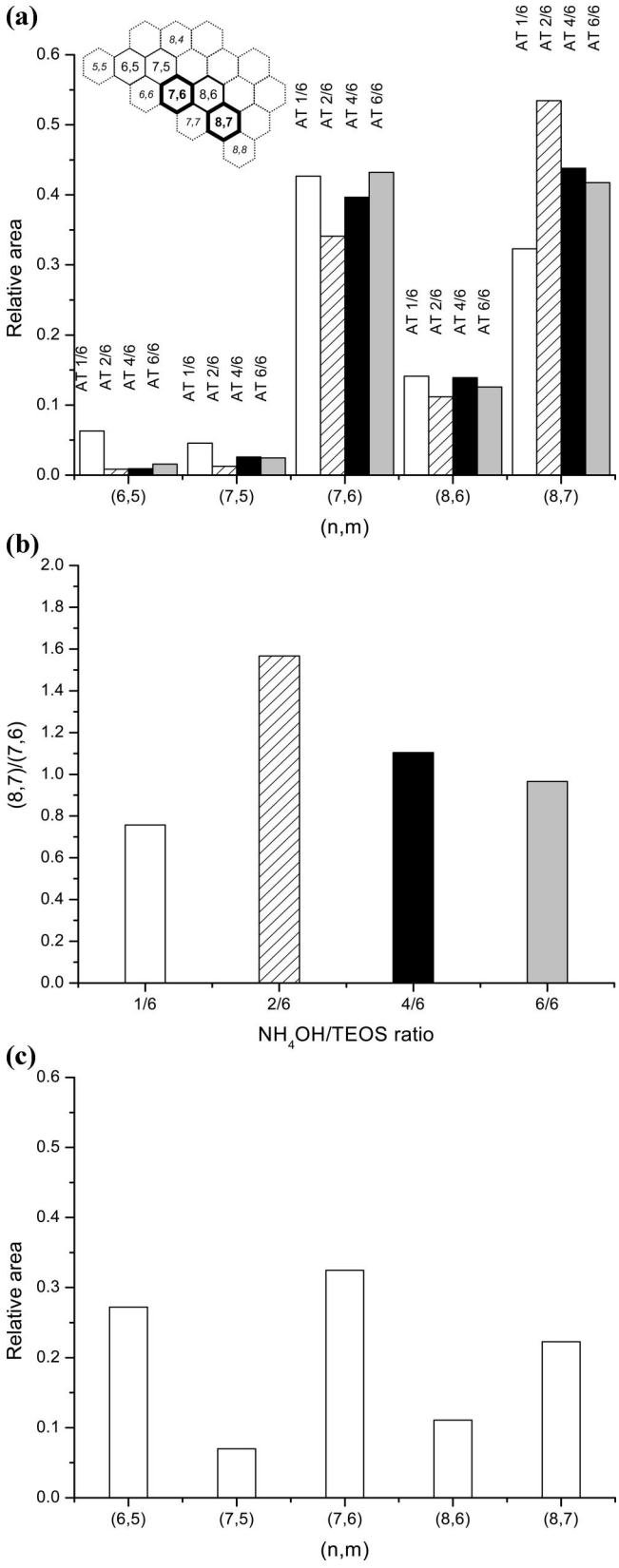

Figure 6. (a) (*n*,*m*) distribution of SWNT grown onto four Co−Mo/SiO_2 powder catalysts with ammonia/TEOS ratios from1/6 to 6/6. (b) Ratio of the two observed main SWNT chiralities (7,6) and (8,7) grown onto four Co−Mo/SiO_2 powder catalysts with ammonia/TEOS ratios from 1/6 to 6/6. (c) (*n*,*m*) distribution of SWNT grown onto a Co−Mo/SiO_2 microstructured catalyst with an ammonia/TEOS ratio of 2/6.

to SWNT, as anticipated from the quality of the Raman spectra. The TEM images also show that the particle sizes

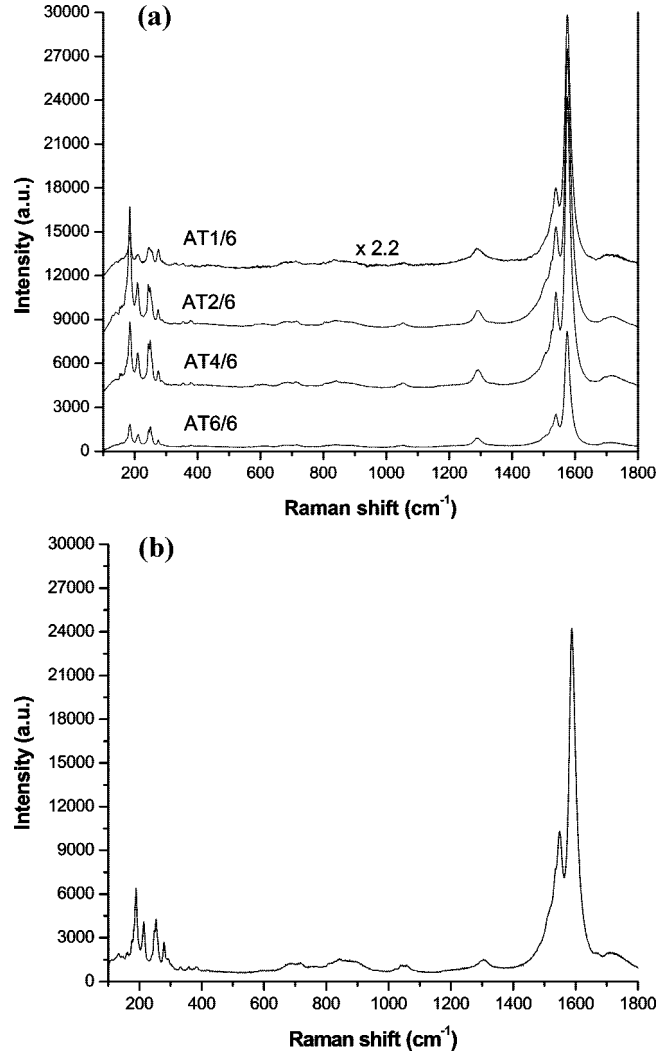

Figure 7. (a) Raman spectra of SWNT grown onto four Co−Mo/SiO_2 powder catalysts with ammonia/TEOS ratios from1/6 to 6/6. (b) Raman spectrum of SWNT grow onto Co−Mo/SiO_2 microstructured catalyst with an ammonia/TEOS ratio of 2/6.

of both the silica support and the Co−Mo moieties increase as the NH_4OH/TEOS ratio increases from 2/6 to 6/6.

Figure 10a,b shows in detail the morphology of the two samples that produce the lowest nanotube yields, AT(1/6) and AT(6/6). It can be seen that while in the latter a large fraction of the Co−Mo particles are surrounded by a silica layer, in the former, the metal particles remain exposed to the gas phase. However, in agreement with the Raman results, the size of these exposed Co−Mo crystallites is comparatively large (∼10 nm). Previous investigations[18] have demonstrated that by increasing the concentration of the hydrolysis catalyst (ammonia, in this case) the average size of the silica particle tends to increase. A rapid increase due to a high concentration of ammonia in the case of sample AT(6/6) may result in encapsulation of the Co−Mo species, as observed. At the other end, when the ammonia concentra-

(30) Herrera, J. E.; Balzano, L.; Pompeo, F.; Resasco, D. E. *J. Nanosci. Nanotechnol.* **2003**, *3*, 1.
(31) Alvarez, W. E.; Pompeo, F.; Herrera, J. E.; Balzano, L.; Resasco, D. E. *Chem. Mater.* **2002**, *14*, 1853.
(32) Reich S.; Thomsen C.; Maultzsch J. *Carbon Nanotubes: Basic concepts and physical properties*; Wiley-VCH: New York, 2004.

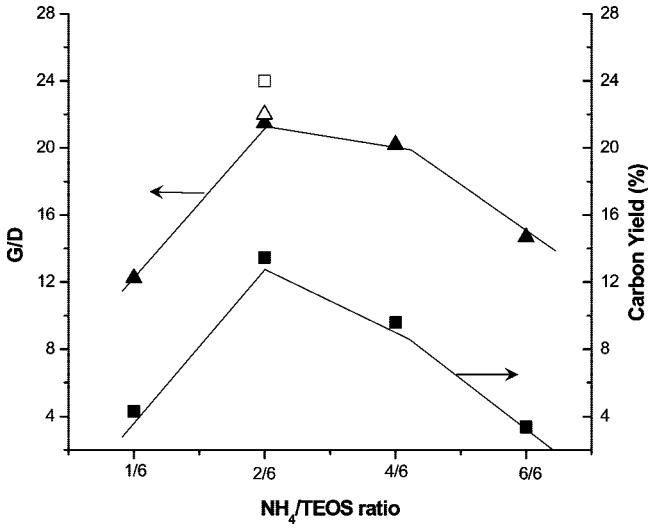

Figure 8. G/D ratios and carbon yields (%) of SWNT grown onto four Co−Mo/SiO_2 powder catalysts with ammonia ratios from 1/6 to 6/6 (G/D ratios (▲) and carbon yield (%) (■)). G/D ratio and carbon yield (%) of SWNT grow onto a microstructured catalyst with an ammonia/TEOS ratio of 2/6 (G/D ratio (△) and carbon yield (%) (□)).

tion is too low, that is, AT(1/6), the extent of polymerization is low and consequently there are not enough silica particles to keep Co−Mo species separate, so they agglomerate during synthesis and produce large crystallites, as clearly seen by TEM and Raman. From the analysis of the carbon yields and Raman G/D ratios shown in Figure 8, it is obvious that both extremes are detrimental for nanotube production yield, as well as nanotube quality. First, if the active species are trapped by the support, one can obviously expect a low carbon yield. Second, large Co−Mo crystallites also have a low fraction of Co exposed to the gas phase, which causes both low yield and low SWNT quality, as previously shown.[5−9] Therefore, in the AT(2/6) sample the concentration of ammonium hydroxide seems to be an optimum, not resulting in large Co−Mo crystallites, which are nonselective and are formed when the extent of silica polymerization is low, nor forming silica-encapsulated Co−Mo moietes, which have low catalytic activity and are formed when the silica polymerization is fast.

Figure 11 shows an SEM image of SWNT grown onto the microscale structured catalyst. It can be seen that the catalyst tubular shape is kept after reaction and that the nanotubes have free space to grow with much less hindrance than on the more compact structure present in the powder catalysts. As a result, the carbon yield is much higher on this open-structure catalyst than on the other catalysts.

3.3.4. Temperature Programmed Oxidation. TPO profiles of the nanotube product obtained over two catalysts with the same NH_4OH/TEOS ratio of 2/6 but prepared by either impregnation or the sol−gel method are compared in Figure 12a. It must be noted that the TPOs are obtained on the as-produced nanotube product; that is, the sample still contains the Co−Mo/SiO_2 catalyst, which certainly may participate in the oxidation process. It is obvious that the oxidation temperatures for the samples prepared by using the sol−gel method with or without template appear at significantly higher temperatures than those on the impregnated catalyst. As discussed before,[26] differences in oxidation temperature

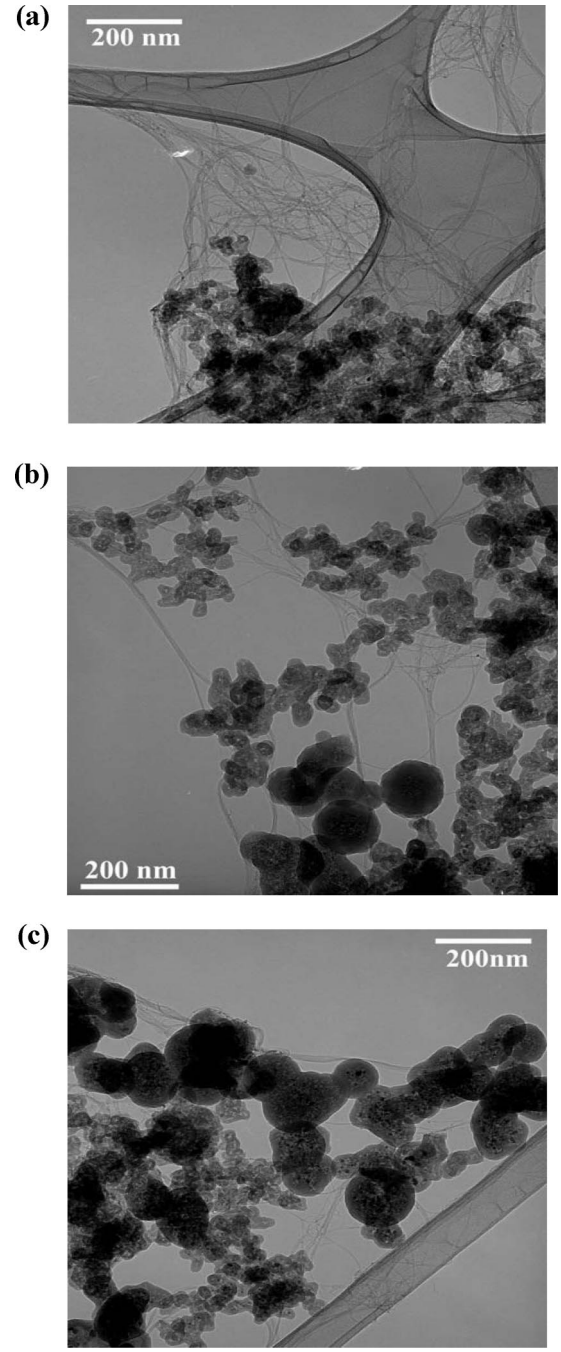

Figure 9. (a) TEM image of SWNT grown onto Co−Mo/SiO_2 powder catalyst with an ammonia/TEOS ratio of 2/6. (b) TEM image of SWNT grown onto Co-Mo/SiO_2 powder catalyst with an ammonia/TEOS ratio of 4/6. (c) TEM image of SWNT grown onto Co−Mo/SiO_2 powder catalyst with an ammonia/TEOS ratio of 6/6.

could indicate the presence of other forms of carbon, such as MWNT or carbon fibers.[6] However, in this case detailed characterization results of the different products by other techniques do not support this explanation. That is, while the AT(2/6) and the microstructured samples have the highest oxidation temperatures they show the highest selectivity toward SWNT. Another possibility for the TPO shifts would be differences in the nanotube diameter. That is, the smaller diameter nanotubes are oxidized at lower temperatures. However, as shown above, while the sol gel catalysts do result in slightly larger diameter than the standard impreg-

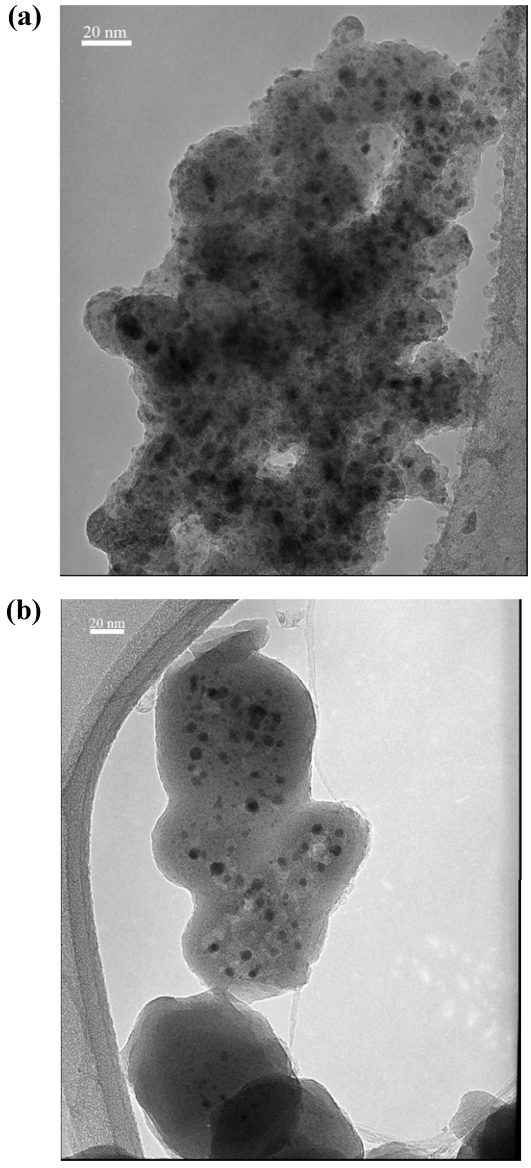

Figure 10. (a) TEM image of SWNT grown onto Co−Mo/SiO_2 powder catalyst with an ammonia/TEOS ratio of 1/6. (b) TEM image of SWNT grown onto Co−Mo/SiO_2 powder catalyst with an ammonia/TEOS ratio of 6/6.

nated catalyst (i.e., standard CoMoCAT), these differences are not so substantial to explain the large shifts in TPO.

It is important to keep in mind that the position of the TPO peaks is greatly affected by the state of aggregation of the nanotubes and the morphology of the catalyst itself. The catalyst morphology and pore structure may affect the fraction of metal surface exposed, the insulating properties of the silica support, and the state of aggregation of the final product, which may affect the kinetics of the oxidation process. At the same time, external heat and mass transfer effects may play a role, and they can vary from one type of support to the other. To further analyze these effects, two additional experiments were conducted. First, the heating ramp was varied. As shown in Figure 12b, when the TPO was conducted at a heating rate of 5 °C/min instead of the standard 10 °C/min, a slight shift to lower temperatures was observed. This shift might indicate a small effect of heat transfer limitations; however, the shift is much smaller than the significant differences observed among the various

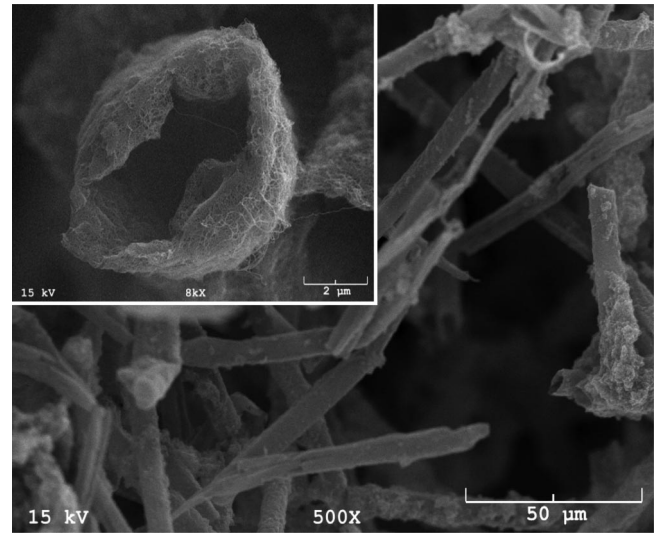

Figure 11. SEM image of the SWNT grown onto Co−Mo/SiO_2 micro-structured catalyst with an ammonia/TEOS ratio of 2/6.

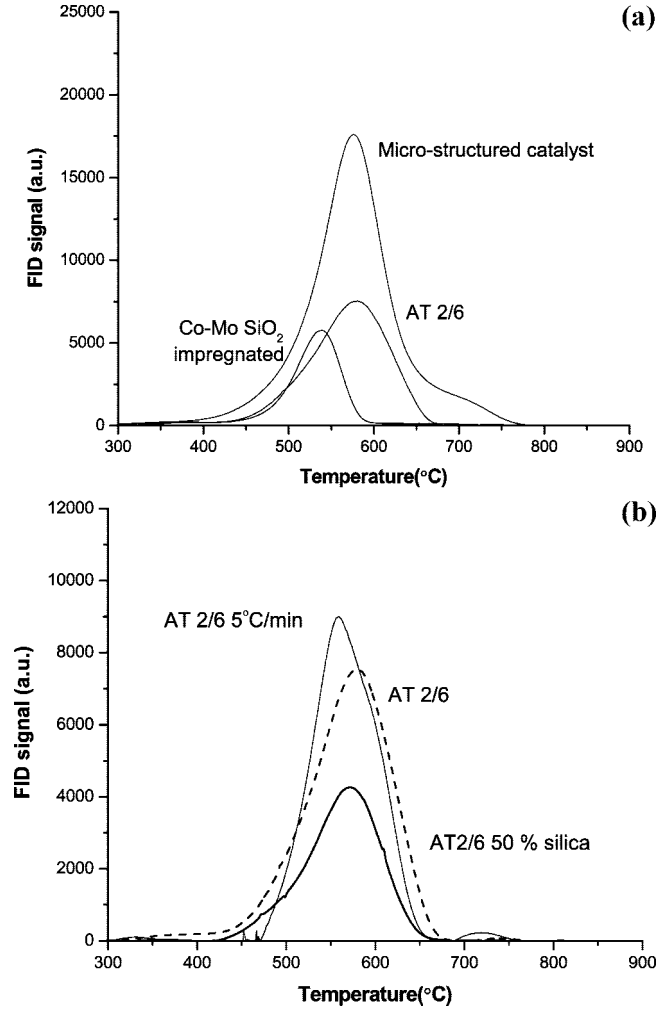

Figure 12. (a) TPO profiles of SWNT grown onto a Co−Mo/SiO_2 impregnated catalyst, onto a sol−gel powder catalyst, and onto a micro-structured catalyst. (b) TPO profiles of SWNT grown onto a Co−Mo/SiO_2 sol−gel powder catalyst oxidized at 5 °C/min and 10 °C/min and a 50−50% SWNT−silica mixture.

catalysts. Similarly, the second additional experiment, in which the powder catalyst (AT2/6) was physically diluted with silica (50−50%), did not show any significant effect.

As shown in Figure 12b, diluting the catalyst in half essentially resulted in a peak of 50% lower intensity, without any significant shift in position. These experiments demonstrate that external heat and mass transfer effects have little influence, and therefore the differences observed in TPO should be related to the internal structure of each individual catalyst particle.

5. Conclusions

We have shown that the sol−gel preparation method has versatility to widely vary the morphology of Co−Mo catalysts used in the synthesis of SWNT. In turn, these changes in morphology result in reproducible changes in nanotube quality and yield. By increasing the ammonia concentration in the sol−gel step, the silica particle size increases as the rates of hydrolysis and polymerization of TEOS are accelerated. Therefore, when the NH_4OH/TEOS ratio is high a large fraction of Co−Mo species remains encapsulated under the silica. By contrast, at low NH_4OH/TEOS ratios, the rate of silica polymerization is low, which results in an enhanced agglomeration of Co and Mo species. Both extremes are detrimental for SWNT production. An optimum preparation is found at intermediate NH_4OH/TEOS ratios.

Acknowledgment. The project was financially supported by the Department of Energy-Basic Energy Sciences (Grants DEFG03-02ER15345 and DE-FG02-06ER64239) and the Oklahoma State Regents for Higher Education. SEM and TEM characterization were conducted in the Samuel Roberts Noble Electron Microscopy Laboratory at the University of Oklahoma.

CM900250K